

Diffraction Physics in ALICE

Proceedings Workshop HERA and the LHC, may 26-30, 2008, CERN

R. Schicker

Physikalisches Inst., Philosophenweg 12, 69120 Heidelberg

Abstract

The ALICE detector at the Large Hadron Collider (LHC) consists of a central barrel, a muon spectrometer and neutron calorimeters at 0° . Additional detectors for event classification and for trigger purposes are placed on both sides of the central barrel. Such a geometry allows the definition of a diffractive gap trigger by requiring no activity in the additional detectors. I discuss some physics topics which become accessible by this gap trigger.

1 The ALICE Experiment

The ALICE experiment is presently being commissioned at the Large Hadron Collider (LHC) [1, 2]. The ALICE experiment consists of a central barrel covering the pseudorapidity range $-0.9 < \eta < 0.9$ and a muon spectrometer in the range $-4.0 < \eta < -2.4$. Additional detectors for trigger purposes and for event classification exist in the range $-4.0 < \eta < 5.0$. The ALICE physics program foresees data taking in pp and PbPb collisions at luminosities up to $\mathcal{L} = 5 \times 10^{30} \text{cm}^{-2} \text{s}^{-1}$ and $\mathcal{L} = 10^{27} \text{cm}^{-2} \text{s}^{-1}$, respectively. An asymmetric system pPb will be measured at a luminosity of $\mathcal{L} = 10^{29} \text{cm}^{-2} \text{s}^{-1}$.

1.1 The ALICE Central Barrel

The detectors in the ALICE central barrel track and identify hadrons, electrons and photons in the pseudorapidity range $-0.9 < \eta < 0.9$. The magnetic field strength of 0.5 T allows the measurement of tracks from very low transverse momenta of about 100 MeV/c to fairly high values of about 100 GeV/c. The tracking detectors are designed to reconstruct secondary vertices resulting from decays of hyperons, D and B mesons. The granularity of the central barrel detectors is chosen such that particle tracking and identification can be achieved in a high multiplicity environment of up to 8000 particles per unit of rapidity. The main detector systems for these tasks are the Inner Tracking System, the Time Projection Chamber, the Transition Radiation Detector and the Time of Flight array. These systems cover the full azimuthal angle within the pseudorapidity range $-0.9 < \eta < 0.9$ and are described below. Additional detectors with partial coverage of the central barrel are a PHOTON Spectrometer (PHOS), an electromagnetic calorimeter (EMCAL) and a High-Momentum Particle Identification Detector (HMPID).

1.1.1 The Inner Tracking System

The Inner Tracking System (ITS) consists of six cylindrical layers of silicon detectors at radii from 4 cm to 44 cm. The minimum radius is determined by the beam pipe dimensions whereas the maximum radius chosen is determined by the necessity of efficient track matching with the outer detectors in the central barrel. The innermost layer extends over the range $-2 < \eta < 2$ such that there is continuous overlap with event classification detectors outside of the central barrel. Due to the high particle density of up to 80 particles/cm² and in order to achieve the required tracking resolution, pixel detectors have been chosen for the first two layers. Silicon drift detectors are located in the middle two layers whereas double sided silicon strip detectors are in the outer two layers.

1.1.2 The Time Projection Chamber

The Time Projection Chamber (TPC) is the main tracking detector in the central barrel. The inner and outer radii of the active volume are 84.5 cm and 246.6 cm, respectively. The full radial track length is

measured in the pseudorapidity range $-0.9 < \eta < 0.9$ whereas tracks with at least one third of nominal radial length are covered in the pseudorapidity range $-1.5 < \eta < 1.5$. Particle identification is achieved by measuring the specific ionization loss. The chosen geometry results in a drift time of about $90 \mu\text{s}$. This long drift time is the factor limiting the proton-proton luminosity to the value mentioned above.

1.1.3 The Transition Radiation Detector

The principal goal of the Transition Radiation Detector (TRD) is to provide electron identification in the momentum range larger than $1 \text{ GeV}/c$. In this range, the electron identification by energy loss in the TPC is no longer sufficient. Since the TRD is a fast tracker, the TRD information can be used for an efficient trigger on high transverse momentum electrons. In addition, the position information from the TRD system improves the tracking performance of the central barrel.

1.1.4 The Time of Flight Detector

The Time-Of-Flight (TOF) array is located at a radial distance from 3.7 m to 4.0 m . The TOF information is used for particle identification in the range $0.2 \text{ GeV}/c < p_T < 2.5 \text{ GeV}/c$. For this detector, the Multi-gap Resistive-Plate (MRPC) technology was chosen. A strip with an active area of $120 \times 7.4 \text{ cm}^2$ consists of pads of 3.5 cm length and 2.5 cm width.

1.1.5 The Central Barrel Performance

The ITS, TPC and TRD detectors described above are the main tracking detectors in the central barrel. With the information from these detectors, particles with momenta as low as $100 \text{ MeV}/c$ can be tracked.

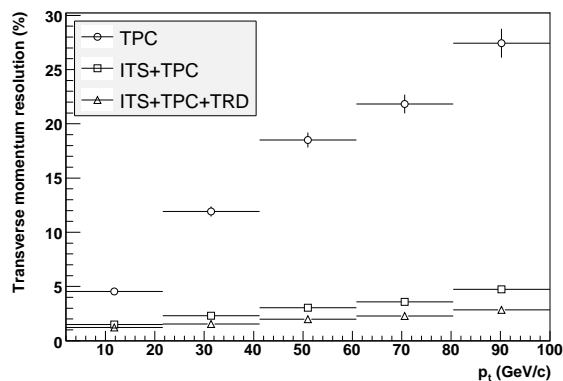


Fig. 1: Central barrel tracking resolution

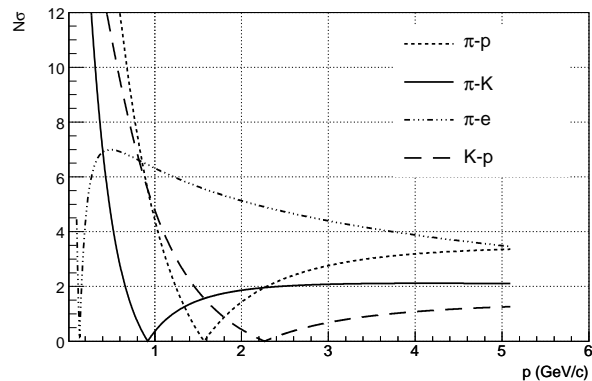


Fig. 2: Particle identification by dE/dx measurement

Fig.1 shows the transverse momentum resolution as expected from simulations. The TPC alone achieves a resolution of approximately 3% at a transverse momentum of $p_T = 10 \text{ GeV}/c$. Adding the information from ITS and TRD on the inner and outer side, respectively, improves the resolution considerably due to the increased leverage. The combined transverse momentum resolution from the ITS, TPC and TRD detector is expected to be about 3% at a transverse momentum of $p_T = 100 \text{ GeV}/c$.

Particle identification is achieved in the central barrel by different methods. The specific energy loss is measured by the TPC, the TRD and the strip and drift detectors of the ITS. Fig.2 shows the combined particle identification capability by dE/dx measurement as a function of momentum. The separation of different particle species is shown in units of the resolution of the dE/dx measurement. The electron-pion separation at high momenta is significantly improved by the information of the TRD system.

1.2 The ALICE Zero Degree Neutron Calorimeter

The Zero Degree Neutron Calorimeters (ZDC) are placed on both sides of the interaction point at a distance of 116 m [3]. The ZDC information can be used to select different diffractive topologies. Events of the type $pp \rightarrow ppX$ do not deposit energy in these calorimeters, events $pp \rightarrow pN^*X$ will have energy in one of the calorimeters whereas events $pp \rightarrow N^*N^*X$ will have energy deposited in both calorimeters. Here, X denotes a centrally produced diffractive state from which the diffractive L0 trigger is derived as described below.

2 The ALICE diffractive gap trigger

Additional detectors for event classification and trigger purposes are located on both sides of the ALICE central barrel. First, an array of scintillator detectors (V0) is placed on both sides of the central barrel. These arrays are labeled V0A and V0C on the two sides, respectively. Each of these arrays covers a pseudorapidity interval of about two units with a fourfold segmentation of half a unit. The azimuthal coverage is divided into eight segments of 45° degrees hence each array is composed of 32 individual counters. Second, a Forward Multiplicity Detector (FMD) is located on both sides of the central barrel. The pseudorapidity coverage of this detector is $-3.4 < \eta < -1.7$ and $1.7 < \eta < 5.1$, respectively.

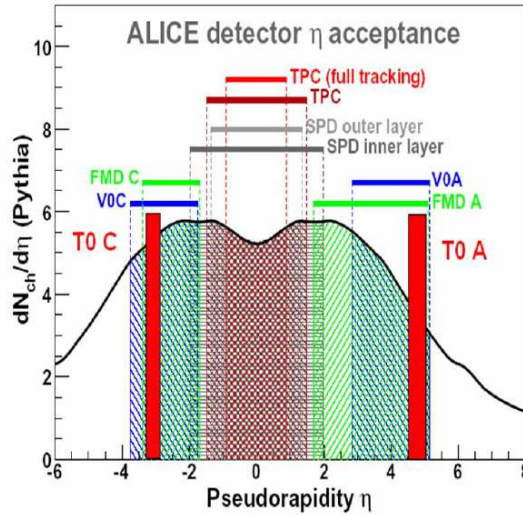


Fig. 3: Pseudorapidity coverage of trigger detectors and of detectors in central barrel

Fig.3 shows the pseudorapidity coverage of the detector systems described above. The geometry of the ALICE central barrel in conjunction with the additional detectors V0 and FMD is well suited for the definition of a rapidity gap trigger. The ALICE trigger system consists of a Central Trigger Processor (CTP) and is designed as a multi-level scheme with L0,L1 and L2 levels and a high-level trigger (HLT). A rapidity gap trigger can be defined by the requirement of signals coming from the central barrel detectors while V0 and FMD not showing any activity. Such a scheme requires a trigger signal from within the central barrel for L0 decision. The pixel detector of the ITS system is suited for delivering such a signal [4]. Alternatively, this L0 signal can be derived from the TOF detector.

The high level trigger HLT has access to the information of all the detectors shown in Fig.3 and will hence be able to select events with rapidity gaps in the range $-4 < \eta < -1$ and $1 < \eta < 5$. These gaps extend over seven units of pseudorapidity and are hence expected to suppress minimum bias inelastic events by many orders of magnitude.

In addition to the scheme described above, the ALICE diffractive L0 trigger signal can be generated from the Neutron ZDC if no central state is present in the reaction. A L0 signal from ZDC does,

however, not arrive at the CTP within the standard L0 time window. A L0 trigger from ZDC is therefore only possible during special data taking runs for which the standard L0 time limit is extended. The possibility of such data taking is currently under discussion.

3 ALICE diffractive physics

The tracking capabilities at very low transverse momenta in conjunction with the excellent particle identification make ALICE an unique facility at LHC to pursue a long term physics program of diffractive physics. The low luminosity of ALICE as compared to the other LHC experiments restricts the ALICE physics program to reactions with cross section at a level of a few nb per unit of rapidity.

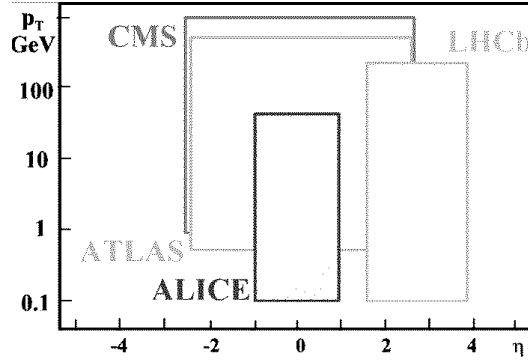


Fig. 4: Rapidity and transverse momentum acceptance of the LHC experiments

Fig.4 shows the transverse momentum acceptance of the four main LHC experiments. Not shown in this figure is the acceptance of the TOTEM experiment which has a physics program of measurements of total cross section, elastic scattering and soft diffraction [5]. The acceptance of the TOTEM telescopes is in the range of $3.1 < |\eta| < 4.7$ and $5.3 < |\eta| < 6.5$. The CMS transverse momentum acceptance of about 1 GeV/c shown in Fig.4 represents a nominal value. The CMS analysis framework foresees the reconstruction of a few selected data samples to values as low as 0.2 GeV/c [6].

4 Signatures of Pomeron

The geometry of the ALICE experiment is suited for measuring a centrally produced diffractive state with a rapidity gap on either side. Such a topology can result, among other, from double Pomeron exchange with subsequent hadronization of the central state. It is expected that the secondaries from Pomeron-Pomeron fusion events show markedly different characteristics as compared to secondaries from inelastic minimum bias events.

First, it is expected that the production cross section of glueball states in Pomeron fusion is larger as compared to inelastic minimum bias events. It will therefore be interesting to study the resonances produced in the central region when two rapidity gaps are required [7].

Second, the slope α' of the Pomeron trajectory is rather small: $\alpha' \sim 0.25 \text{ GeV}^{-2}$ in DL fit and $\alpha' \sim 0.1 \text{ GeV}^{-2}$ in vector meson production at HERA [8]. These values of α' in conjunction with the small t-slope ($< 1 \text{ GeV}^{-2}$) of the triple Pomeron vertex indicate that the mean transverse momentum k_t in the Pomeron wave function is relatively large $\alpha' \sim 1/k_t^2$, most probably $k_t > 1 \text{ GeV}$. The transverse momenta of secondaries produced in Pomeron-Pomeron interactions are of the order of this k_t . Thus the mean transverse momenta of secondaries produced in Pomeron-Pomeron fusion is expected to be larger as compared to inelastic minimum bias events.

Third, the large k_t described above corresponds to a large effective temperature. A suppression of strange quark production is not expected. Hence the K/ π ratio is expected to be enhanced in Pomeron-

Pomeron fusion as compared to inelastic minimum bias events [9]. Similarly, the η/π and η'/π ratios are expected to be enhanced due to the hidden strangeness content and due to the gluon components in the Fock states of η, η' .

5 Signatures of Odderon

The Odderon was first postulated in 1973 and is represented by color singlet exchange with negative C-parity [10]. Due to its negative C-parity, Odderon exchange can lead to differences between particle-particle and particle-antiparticle scattering. In QCD, the Odderon can be a three gluon object in a symmetric color state. Due to the third gluon involved in the exchange, a suppression by the coupling α_s is expected as compared to the two gluon Pomeron exchange. However, finding experimental signatures of the Odderon exchange has so far turned out to be extremely difficult [11]. A continued non-observation of Odderon signatures would put considerable doubt on the formulation of high energy scattering by gluon exchange [12]. The best evidence so far for Odderon exchange was established as a difference between the differential cross sections for elastic pp and $p\bar{p}$ scattering at $\sqrt{s} = 53$ GeV at the CERN ISR. The pp cross section displays a dip at $t = -1.3$ GeV² whereas the $p\bar{p}$ cross section levels off. Such a behaviour is typical for negative C-exchange and cannot be due to mesonic Reggeons only.

5.1 Signatures of Odderon Cross Sections

Signatures of Odderon exchanges can be looked for in exclusive reactions where the Odderon (besides the Photon) is the only possible exchange. Diffractively produced C-even states such as pseudoscalar or tensor mesons can result from Photon-Photon, Photon-Odderon and Odderon-Odderon exchange. Any excess measured beyond the well understood Photon-Photon contribution would indicate an Odderon contribution.

Diffractively produced C-odd states such as vector mesons $\phi, J/\psi, \Upsilon$ can result from Photon-Pomeron or Odderon-Pomeron exchange. Any excess beyond the Photon contribution would be indication of Odderon exchange.

Estimates of cross section for diffractively produced J/ψ in pp collisions at LHC energies were first given by Schäfer et al [13]. More refined calculations by Bzdak et al result in a t-integrated photon contribution of $\frac{d\sigma}{dy} |_{y=0} \sim 15$ nb and a t-integrated Odderon contribution of $\frac{d\sigma}{dy} |_{y=0} \sim 1$ nb [14]. These two numbers carry large uncertainties, the upper and lower limit of these numbers vary by about an order of magnitude. This cross section is, however, at a level where in 10⁶ s of ALICE data taking the J/ψ can be measured in its e^+e^- decay channel at a level of 4% statistical uncertainty.

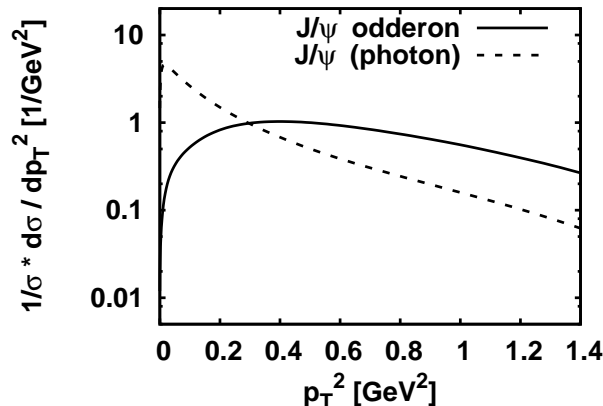


Fig. 5: The J/ψ transverse momentum distribution for the photon and Odderon contributions

Due to the different t -dependence, the Photon and Odderon contribution result in different transverse momentum distribution p_T of the J/ψ . The photon and Odderon contributions are shown in Fig.5 by the dotted and solid lines, respectively. A careful transverse momentum analysis of the J/ψ might therefore allow to disentangle the Odderon contribution.

5.2 Signatures of Odderon Interference Effects

If the diffractively produced final state is not an eigenstate of C-parity, then interference effects between photon-Pomeron and photon-Odderon amplitudes can be analyzed.

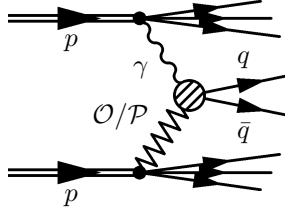


Fig. 6: photon-Pomeron and photon-Odderon amplitudes

Fig.6 shows the photon-Pomeron and the photon-Odderon amplitudes for $q\bar{q}$ production. A study of open charm diffractive photoproduction estimates the asymmetry in fractional energy to be on the order of 15% [15]. The forward-backward charge asymmetry in diffractive production of pion pairs is calculated to be on the order of 10% for pair masses in the range $1 \text{ GeV}/c^2 < m_{\pi^+\pi^-} < 1.3 \text{ GeV}/c^2$ [16, 17].

6 Photoproduction of heavy quarks

Diffractive reactions involve scattering on small- x gluons in the proton. The number density of gluons at given x increases with Q^2 , as described by the DGLAP evolution. Here, Q^2 and x denote the kinematical parameters used in deep inelastic ep scattering. The transverse gluon density at a given Q^2 increases with decreasing x as described by the BFKL evolution equation. At some density, gluons will overlap and hence reinteract. In this regime, the gluon density saturates and the linear DGLAP and BFKL equation reach their range of applicability. A saturation scale $Q_s(x)$ is defined which represents the breakdown of the linear regime. Nonlinear effects become visible for $Q < Q_s(x)$.

Diffractive heavy quark photoproduction represents an interesting probe to look for gluon saturation effects at LHC. The inclusive cross section for $Q\bar{Q}$ photoproduction can be calculated within the dipole formalism. In this approach, the photon fluctuates into a $Q\bar{Q}$ excitation which interacts with the proton as a color dipole. The dipole cross section $\sigma(x,r)$ depends on x as well as on the transverse distance r of the $Q\bar{Q}$ pair. A study of inclusive heavy quark photoproduction in pp collisions at LHC energy has been carried out [18]. These studies arrive at differential cross sections for open charm photoproduction of $\frac{d\sigma}{dy} |_{y=0} \sim 1.3 \mu\text{b}$ within the collinear pQCD approach as compared to $\frac{d\sigma}{dy} |_{y=0} \sim 0.4 \mu\text{b}$ within the color glass condensate (CGC). The cross sections are such that open charm photoproduction seems measurable with good statistical significance. The corresponding numbers for the cross section for bottom photoproduction are $\frac{d\sigma}{dy} |_{y=0} \sim 20 \text{ nb}$ and 10 nb , respectively.

Diffractive photoproduction is characterized by two rapidity gaps in the final state. In the dipole formalism described above, the two gluons of the color dipole interaction are in color singlet state. Diffractive heavy quark photoproduction cross sections in pp, pPb and PbPb collisions at LHC have been studied [19]. The cross sections for diffractive charm photoproduction are $\frac{d\sigma}{dy} |_{y=0} \sim 6 \text{ nb}$ in pp, $\frac{d\sigma}{dy} |_{y=0} \sim 9 \mu\text{b}$ in pPb and $\frac{d\sigma}{dy} |_{y=0} \sim 11 \text{ mb}$ in PbPb collisions. The corresponding numbers for

diffractive bottom photoproduction are $\frac{d\sigma}{dy} |_{y=0} \sim 0.014$ nb in pp, $\frac{d\sigma}{dy} |_{y=0} \sim 0.016$ μ b in pPb and $\frac{d\sigma}{dy} |_{y=0} \sim 0.02$ mb in PbPb collisions.

Heavy quarks with two rapidity gaps in the final state can, however, also be produced by central exclusive production, i.e. two Pomeron fusion. The two production mechanisms have a different t -dependence. A careful analysis of the transverse momentum p_T of the $Q\bar{Q}$ pair might therefore allow to disentangle the two contributions.

Acknowledgments

I thank Otto Nachtmann and Carlo Ewerz for illuminating discussions and Leszek Motyka for preparing and communicating Figure 5.

References

- [1] F. Carminati et al, ALICE Collaboration, 2004, J.Phys. G: Nucl. Part. Phys. **30** 1517
- [2] B. Alessandro et al, ALICE Collaboration, 2006, J.Phys. G: Nucl. Part. Phys. **32** 1295
- [3] R. Arnaldi et al, Nucl. Instr. and Meth. A **564** (2006) 235
- [4] The ALICE collaboration, K. Aamodt et al., The ALICE experiment at the CERN LHC, 2008_JINST_3_S08002.
- [5] K. Eggert, TOTEM a different LHC experiment, CERN colloquium, feb 21,2008
- [6] D. d'Enterria et al, Addendum CMS technical design report, J. Phys. G34:2307-2455, 2007
- [7] F. Close, A. Kirk, G. Schuler, Phys.Lett. B **477** (2000) 13
- [8] A. Donnachie, P. Landshoff, Phys.Lett. B**595** (2004) 393
- [9] T. Åkesson et al, Nucl. Phys. B **264** (1986) 154
- [10] L. Lukaszuk, B. Nicolescu, Lett. Nuovo Cim. **8** (1973) 406
- [11] C. Ewerz, Proceedings XII Rencontres de Blois (2005) 377
- [12] S. Donnachie, G. Dosch, P.V. Landshoff, O. Nachtmann, Pomeron physics and QCD, Cambridge University Press (2002) 297
- [13] A. Schäfer, L. Mankiewicz, O. Nachtmann, Phys.Lett. B **272** (1991) 419
- [14] A. Bzdak, L. Motyka, L. Szymanowski, J.R. Cudell, Phys.Rev. D **75** (2007) 094023
- [15] S.J. Brodsky, J. Rathsman, C. Merino, Phys.Lett. B **461** (1999) 114
- [16] P. Hägler, B. Pire, L. Szymanowski, O.V. Teryaev, Phys.Lett. B **535** (2002) 117
- [17] I.F. Ginzburg, I.P. Ivanov, N.N. Nikolaev, Eur.Phys.J. C**5** (2003) 02
- [18] V.P. Goncalves, M.V. Machado, Phys.Rev.D **71** (2005) 014025
- [19] V.P. Goncalves, M.V. Machado, Phys.Rev.D **75** (2007) 031502